Antiviral Research 106 (2014) 61–70

Contents lists available at ScienceDirect

Antiviral Research

journal homepage: www.elsevier.com/locate/antiviral

Assessment of Dengue virus helicase and methyltransferase as targets for fragment-based drug discovery

Bruno Coutard [a,b], Etienne Decroly [a,b], Changqing Li [a,b], Andrew Sharff [c], Julien Lescar [a,b], Gérard Bricogne [c], Karine Barral [a,b,*]

[a] Aix-Marseille Université, AFMB UMR 7257, 163 Avenue de Luminy, Case 932, 13288 Marseille Cedex 09, France
[b] CNRS, AFMB UMR 7257, 163 Avenue de Luminy, Case 932, 13288 Marseille Cedex 09, France
[c] Global Phasing Ltd, Sheraton House, Castle Park, Cambridge CB3 0AX, England, United Kingdom

ARTICLE INFO

Article history:
Received 10 December 2013
Revised 14 March 2014
Accepted 18 March 2014
Available online 1 April 2014

Keywords:
Dengue virus
NS5 methyltransferase
NS3 helicase
Fragment-based drug discovery
Antiviral screening

ABSTRACT

Seasonal and pandemic flaviviruses continue to be leading global health concerns. With the view to help drug discovery against Dengue virus (DENV), a fragment-based experimental approach was applied to identify small molecule ligands targeting two main components of the flavivirus replication complex: the NS3 helicase (Hel) and the NS5 mRNA methyltransferase (MTase) domains. A library of 500 drug-like fragments was first screened by thermal-shift assay (TSA) leading to the identification of 36 and 32 fragment hits binding Hel and MTase from DENV, respectively. In a second stage, we set up a fragment-based X-ray crystallographic screening (FBS-X) in order to provide both validated fragment hits and structural binding information. No fragment hit was confirmed for DENV Hel. In contrast, a total of seven fragments were identified as DENV MTase binders and structures of MTase-fragment hit complexes were solved at resolution at least 2.0 Å or better. All fragment hits identified contain either a five- or six-membered aromatic ring or both, and three novel binding sites were located on the MTase. To further characterize the fragment hits identified by TSA and FBS-X, we performed enzymatic assays to assess their inhibition effect on the N7- and 2′-*O*-MTase enzymatic activities: five of these fragment hits inhibit at least one of the two activities with IC_{50} ranging from 180 μM to 9 mM. This work validates the FBS-X strategy for identifying new anti-flaviviral hits targeting MTase, while Hel might not be an amenable target for fragment-based drug discovery (FBDD).

This approach proved to be a fast and efficient screening method for FBDD target validation and discovery of starting hits for the development of higher affinity molecules that bind to novel allosteric sites.

1. Introduction

Flavivirus infections, such as those caused by mosquito-borne Dengue, West Nile, Kunjin, Japanese encephalitis and Yellow fever viruses, can provoke life-threatening diseases of epidemic proportions with a devastating economic impact. The Dengue virus (DENV) itself causes 50–100 million human infections annually, leading to about 30,000 deaths; its transmission has increased dramatically and has become a major international public health concern. Despite recent studies in vaccine development (Thomas and Endy, 2013), there are currently neither a truly cross-protective vaccine nor approved antiviral compounds to treat DENV infections. In such a context, the deployment of an innovative drug discovery approach towards the development of potent antiviral compounds to prevent or treat DENV infections represents an urgent complement to any vaccination campaign.

A natural target is the flaviviral replication machinery, many steps of which have been characterized, leading to the identification of enzymes whose inhibition could block viral replication (Bollati et al., 2010). Flavivirus are single-stranded positive RNA viruses carrying a cap-1 structure ($^{7Me}GpppA_{2'OMe}$-RNA) at their

Abbreviations: DENV, Dengue virus; NS, non-structural protein; MTase, methyltransferase; Hel, helicase; AdoMet, *S*-adenosyl-L-methionine; AdoHcy, *S*-adenosyl-L-homocysteine; FBDD, fragment-based drug discovery; FBS, fragment-based screening; FBS-X, FBS by X-ray crystallography; LE, ligand efficiency; MW, molecular weight; ITC, isothermal titration calorimetry; SPR, surface plasmon resonance; TSA, thermal-shift assay; MS, mass spectrometry; NMR, nuclear magnetic resonance; HCS, high-concentrated screening bioassay; AMPPNP, Adenosine 5′-(β,γ-imido) triphosphate; DTT, dithiothreitol; PEG, polyethylene glycol; SPA, scintillation proximity assay; HTS, high-throughput screening; IC_{50}, inhibitory concentration that causes 50% reduction in enzyme activity; SD, standard deviation.

* Corresponding author at: Aix-Marseille Université, AFMB UMR 7257, 163 Avenue de Luminy, Case 932, 13288 Marseille Cedex 09, France. Tel.: +33 491825581; fax: +33 491266720.
E-mail address: karine.barral@afmb.univ-mrs.fr (K. Barral).

http://dx.doi.org/10.1016/j.antiviral.2014.03.013
0166-3542/

5′-end. The replication of the genome is ensured by the viral replication/transcription complex, composed of five non structural proteins (NS1–NS5) carrying the polymerase, RNA unwinding and capping activities. The flaviviral proteins NS3 and NS5 are carrying two essential enzymatic activities, namely helicase (Hel) and methyltransferase (MTase) that are strictly required for the replication of flaviviruses, and therefore constitute promising targets for the development of anti-flaviviral compounds.

DENV Hel, located at the C-terminal part of NS3, carries nucleotide and RNA triphosphatase (respectively named NTPase and RTPase) as well as RNA unwinding activities (Benarroch et al., 2004b; Yon et al., 2005) involved in RNA capping and viral genome replication, respectively. The inhibition of these functions limits viral replication (Byrd et al., 2013; Daffis et al., 2010; Mastrangelo et al., 2012). DENV NS5 MTase catalyses two consecutive methylation reactions involved in the synthesis of the cap structure: methylation of the cap guanine at its N7-position to yield ^{7Me}GpppA-RNA and methylation of the first transcribed nucleotide at its 2′-*O*-position to yield ^{7Me}GpppA$_{2'OMe}$-RNA (Dong et al., 2008, 2010). Recent biochemical studies coupled to reverse genetic analysis have demonstrated that the N7-MTase activity is essential for the replication of flavivirus (Dong et al., 2010; Zust et al., 2011). By contrast, 2′-*O*-MTase defective viruses can replicate but are highly attenuated (Zust et al., 2013). Thus, both N7- and 2′-*O*-MTase activities are important on the context of antiviral research.

The identification of suitable new target sites and/or starting-point compounds for the development of new anti-flavivirals remains a major challenge (Lim et al., 2013b). In such a perspective, we decided to use a promising drug discovery strategy, namely fragment-based drug discovery (FBDD), now established as a powerful method for the rapid identification of starting hits and their subsequent elaboration into quality lead compounds (Congreve et al., 2008; de Kloe et al., 2009; Erlanson, 2012; Hajduk and Greer, 2007; Murray and Rees, 2009; Scott et al., 2012). This methodology offers an attractive alternative to conventional screening approaches such as HTS. Indeed, the fragment-based screening (FBS) approach has advantages over other lead discovery methods, including the screening of substantially fewer compounds (usually several hundred to a thousand), higher hit rates, a more efficient coverage of the chemical space and a faster fragment hit-to-lead optimization phase. Because of their small size (MW < 300 Da), fragments normally bind with low affinity, however binding is often of high quality as estimated by ligand efficiency (LE) (Abad-Zapatero, 2007; Bembenek et al., 2009; Hopkins et al., 2004). A major challenge in establishing fragment-based screening has been the development of sufficiently sensitive methods to detect weakly binding hits which have typically milli- to micromolar binding affinities (Ciulli and Abell, 2007; Kuo, 2011; Lundqvist, 2005; Siegal et al., 2007). Biophysical methods, such as isothermal titration calorimetry (ITC), surface plasmon resonance (SPR), thermal-shift assay (TSA), mass spectrometry (MS) and nuclear magnetic resonance (NMR), are frequently employed as a first-pass screen before detailed structural characterization by X-ray crystallography (FBS-X). Knowledge of exactly how the fragments bind to the protein target allows the hits to be extended into neighboring pockets to create higher affinity and more specific compounds.

In the past decade, several crystal structures of NS3 DENV Hel (Luo et al., 2008, 2010; Xu et al., 2005) and NS5 DENV MTase (Benarroch et al., 2004a; Egloff et al., 2002, 2007; Geiss et al., 2009; Lim et al., 2011; Yap et al., 2010) have been reported. Crystal forms diffracting to better than 2 Å resolution have been identified (Lim et al., 2011; Luo et al., 2008) and are suitable for determining the co-crystal structures that would provide the molecular basis for downstream ligand optimization. We have therefore applied an FBS approach targeting the NS3 DENV Hel and NS5 DENV MTase domains to discover starting-point compounds for further antiviral development. In this study, we set up a multistep fragment-based screening strategy involving both interaction and enzymatic inhibition analyses. A library of 500 fragments was successively screened by thermal-shift assay allowing the initial selection of fragments that bind to NS3 DENV Hel and NS5 DENV MTase domains, with some of them showing inhibition effect on activity assays. We then successfully identified novel binding sites for NS5 DENV MTase using X-ray crystallography.

2. Materials and methods

2.1. Materials

The 500-compound general fragment library was purchased from Maybridge (RO3 library 2009). ATP was purchased from New Englands BioLabs Inc. [^{3}H]AdoMet (80.7 Ci/mmol) was purchased from PerkinElmer. The fluorescent dye SYPRO Orange was purchased from Life Technologies. All other chemicals were purchased from Sigma–Aldrich.

2.2. Production of recombinant proteins

The DNA fragments coding for DENV4 Hel (amino acid region 172–618) and DENV3 MTase (amino acid region 1–277) were synthesized by Geneart (Life Technologies). The coding sequences were cloned in pMcox20A by Gateway recombination, downstream a cleavable Hexahistidine–Thioredoxin tag using a two step PCR protocol. *Escherichia coli* Rosetta (DE3) pLysS (Novagen) were co-transformed with the two plasmids and cultured in Terrific Broth at 37 °C. When OD_{600nm} reached 0.5, expression was induced by adding 500 μM of isopropyl-β-D-1-thiogalactopyranoside (IPTG) in the culture media and temperature was shifted to 25 and 17 °C for DENV3 MTase and DENV4 Hel, respectively. Protein purification and tag removal was performed in non denaturing conditions as previously described (Lantez et al., 2011). A final Size Exclusion Chromatography step was performed in 20 mM Tris–HCl, 200 mM NaCl, glycerol 10%, 2 mM DTT, pH 7.5 for DENV3 MTase and 10 mM Hepes 300 mM NaCl pH7.5 for DENV4 Hel. Dialysis could then be performed to exchange the buffer depending on the downstream experiment.

2.3. Thermal-shift assays (TSA) and data analysis

The thermal-shift assays were conducted in 96-well thin-wall PCR plates (Bio-Rad) sealed with Optical-Quality Sealing tape (Bio-Rad) and heated with an iCycler iQ real Time Detection System (Bio-Rad) from 20 to 90 °C in increments of 0.2 °C. Thermal denaturation was monitored using SYPRO Orange (Life Technologies) and the fluorescence intensity was measured at 490/530 nm excitation/emission wavelengths, respectively. The denaturation of the proteins was monitored by following the increase of the fluorescence emitted by the probe that binds exposed hydrophobic regions of the denatured protein. The melting temperature (T_m) was calculated as the mid-log of the transition phase from the native to the denatured protein using a Boltzmann model (Origin software). The reference unfolding temperature of proteins in 2% DMSO (T_{mref}) was subtracted from the values in the presence of fragment (T_{mfrag}) to obtain thermal shifts, $\Delta T_m = T_{mfrag} - T_{mref}$. Fragments were considered to be hits when $\Delta T_m > 0.5$ °C.

2.3.1. Fragment-based screening against DENV4 Hel by TSA

TSA plates were prepared by dispensing into each well the DENV4 Hel (final concentration of 20 μM in 50 mM HEPES, 150 mM NaCl, 2 mM $MnCl_2$, pH 7.4) which was mixed with 0.5 μL of fragments (from 100 mM stock in 100% DMSO, to attain

a 2 mM final concentration in 2% DMSO) and a SYPRO orange solution in concentrations recommended by the manufacturer in a final volume of 25 μL. Adenosine 5′-(β,γ-imido) triphosphate (AMPPNP) was used in this assay as positive control (0.5 μL at a final concentration of 2 mM).

2.3.2. Fragment-based screening against DENV3 MTase by TSA

TSA plates were prepared by dispensing into each well the DENV3 MTase (final concentration of 40 μM in 10 mM HEPES, 300 mM NaCl, pH 7.5) which was mixed with 0.5 μL of fragment (from 100 mM stock in 100% DMSO, 2 mM final concentration in 2% DMSO) and a SYPRO orange solution in concentrations recommended by the manufacturer in a final volume of 25 μL. *S*-Adenosyl-L-methionine (AdoMet) was used in this assay as positive control (0.5 μL at a final concentration of 2 mM).

2.4. Fragment-based screening by X-ray crystallography (FBS-X)

2.4.1. Crystallization of NS3 DENV4 Hel domain and fragment soaking

The crystallization of NS3 DENV4 Hel domain was performed by the hanging drop vapor diffusion method in 24-well Linbro plates for ease of soaking at 20 °C by mixing 1 μL of protein solution at 2.5 mg/mL (20 mM Tris–HCl, 150 mM NaCl, 2 mM DTT, 5% glycerol, pH 7.4) with 1 μL of reservoir solution (10% PEG 3350 and 100 mM Tris–HCl, pH 7.0). Crystals appeared within 2 days. For fragment soaking experiments, crystals were transferred to 2 μL soaking drops of the reservoir mixture with 10% fragment stock solution (100–500 mM in 100% DMSO). When low solubility of the fragment was problematic, saturated solutions were used. Crystals were soaked between 4 h and 8 h at 20 °C, transferred to a cryoprotectant solution of the same ligand/reservoir solution containing 20% glycerol for a few seconds and flash-cooled in liquid nitrogen.

2.4.2. Crystallization of NS5 DENV3 MTase domain and fragment soaking

The crystallization of NS5 DENV3 MTase domain was performed by the hanging drop vapor diffusion method in 24-well Linbro plates for ease of soaking at 20 °C by mixing 1 μL of protein solution at 8.5 mg/mL (20 mM Tris–HCl, 200 mM NaCl, 2 mM DTT, 10% glycerol, pH 7.4) with 1 μL of reservoir solution (25% PEG 8000, 100 mM Tris, 200 mM NaCl, 20 mM trisodium citrate, pH 8.5). Crystals appeared within 2 days. For fragment soaking experiments, crystals were transferred to 2 μL soaking drops of the reservoir mixture with 10% fragment stock solution (100–500 mM in 100% DMSO). When low solubility of the fragment was problematic, saturated solutions were used. Crystals were soaked between 8 h and overnight, transferred to a cryoprotectant solution of the same ligand/reservoir solution containing 10% glycerol for a few seconds and flash-cooled in liquid nitrogen.

2.4.3. Data collection, automated data processing and refinement

Diffraction data were collected at the European Synchrotron radiation Facility (ID14-4, ID23-1, and ID29) and at SOLEIL synchrotron (Proxima 1). We used Pipedream (Sharff et al., 2011), a tool specifically designed for automating FBS-X by linking data processing with AutoPROC (Vonrhein et al., 2011), rigid-body replacement with Phaser (McCoy et al., 2007), structure refinement with autoBUSTER (Bricogne et al., 2011) and automated ligand fitting with Rhofit (Womack et al., 2011), to facilitate the (high-throughput) fragment screening pathway. Using this automated pipeline, images were processed and scaled using XDS (Kabsch, 2010) and SCALA (Evans, 2006). The structures of free DENV4 NS3 Hel (PDB code 2JLQ) and DENV3 NS5 MTase/AdoMet (PDB code 3P97) were used as template models in the limited molecular replacement procedure. Iterative cycles of model building were done with the program COOT (Emsley et al., 2010). Fragment restraints were generated with grade (Smart et al., 2011) and Mogul (Bruno et al., 2004) using RM1 semi-empirical QM methods. The quality of the refined structures was assessed with MOLPROBITY (Davis et al., 2007). The crystal structures were determined at resolutions between 1.7–2.5 Å for NS3 DENV4 Hel and 1.5–1.9 Å for NS5 DENV3 MTase. These resolution ranges are quite adequate to provide clear electron densities enabling the unequivocal placement of the fragments in their respective structures.

2.5. ATPase-assay with DENV4 Hel

ATPase activity was determined using a direct colorimetric assay as previously described (Henkel et al., 1988) and adapted to 96-well plates (Papageorgiou et al., 2010). Briefly, the ATPase assay was carried out in a 50 μL reaction volume, containing 50 mM Tris–HCl pH 7.5, 2 mM $MgCl_2$, 100 mM NaCl, 0.05 mg/mL BSA, 2 mM DTT, 5% DMSO and 50 nm of DENV4 Hel. The reaction was initiated by the addition of ATP to a final concentration of 0.5 mM and then incubated at 37 °C for 10 min. The reaction was stopped by the addition of EDTA to a final concentration of 20 mM. The colorimetric assay was performed by adding 60 μL of dye solution (12% ascorbic acid in 1 M HCl and l% ammonium molybdate tetrahydrate in H_2O were freshly mixed in a 2:1 ratio) to 20 μL of reaction solution for 5 min incubation. Then 60 μL of 2% sodium citrate in 2% acetic acid was added and the absorbance at 590 nm (A_{590nm}) was measured after 5 min. The concentration of inorganic phosphate was determined by matching A_{590nm} in a standard curve of A_{590nm} versus known standard phosphate concentrations. Fragments were added to the reaction mixture at a final concentration of 2 mM before adding ATP.

2.6. N7- and 2′-O-MTase inhibition testing and data analysis

The characterization of *in vitro* DENV3 N7- and 2′-*O*-MTase activities was previously described in Barral et al., 2013. Briefly, DENV3 2′-*O*-MTase activity was assayed by incubating DENV3 MTase with a selected fragment and a small capped RNA substrate $^{7Me}GpppAC_4$ in the presence of [^{3}H]AdoMet (Milani et al., 2009; Selisko et al., 2010). The MTase activity assay was performed in 20 μL samples containing 40 mM Tris–HCl pH 7.5, 5 mM DTT, 10 μM AdoMet (0.2–2 μCi [^{3}H]AdoMet), 1 μM of DENV3 MTase, 0.5–1 mM of fragment (stock solutions 100 mM in 100% DMSO) and 1 μM $^{7Me}GpppAC_4$. The enzyme, buffer and fragments were first mixed together and the reaction was started with a premix of AdoMet and capped RNA substrates. Reactions were incubated at 30 °C for 30 min and stopped by 20-fold dilution in an ice–cold 100 μM AdoHcy solution. Samples were then transferred onto a DEAE membrane (DEAE Filtermat; Wallac) by a Filtermat Harvester (Packard Instruments) washed with 0.01 M ammonium formate (pH 8.0), water and ethanol, and the radioactivity transferred onto RNA was measured using a Wallac 1450 MicroBeta Trilux Liquid Scintillation Counter. DENV3 N7-MTase activity was performed as described above but using 0.5 μM $GpppA_{2'OMe}$-RNA_{74} as substrate (Barral et al., 2013).

Compounds showing MTase inhibition were next tested using decreasing inhibitor concentration (with twofold serial dilutions) in order to determine the inhibitor concentration at 50% activity (IC_{50}). DENV3 MTase assays were performed as described above. The final concentration of DMSO in reaction mixtures was below 5%. All data points were measured in duplicate. The IC_{50} values were determined using Prism software and adjusted to a logistic dose–response function:% activity = $100/(1 + [I]/IC_{50})^b$, where b corresponds to the slope factor and $[I]$ to inhibitor concentration (Delean et al., 1978).

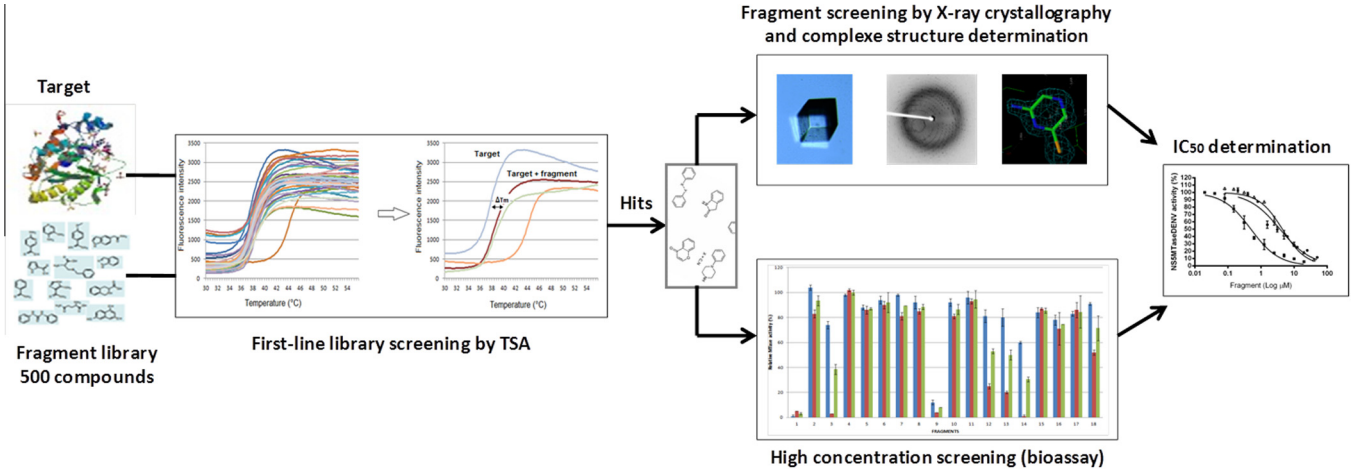

Fig. 1. Fragment-based screening campaign against NS3 Dengue helicase and NS5 Dengue methyltransferase and ligand discovery.

Table 1
Biophysical and activity data on fragment hits.

Fragments	DENV Hel ΔT_m[a] (TSA)	DENV Hel ATPase-assay% inhibition[b]	Fragments	DENV MTase ΔT_m[a] (TSA)	DENV 2′*O*-MTase activity% inhibition[c]	DENV N7-MTase activity% inhibition[d]	DENV 2′*O*-MTase activity IC_{50}[e] (mM)	DENV N7-MTase activity IC_{50}[e] (mM)
1	1.14 ± 0.35	29	**16**	0.98 ± 0.34	0	28	–	–
5	0.73 ± 0.01	47	**17**	0.61 ± 0.14	4	0	–	–
7	0.88 ± 0.23	0	**21**	0.87 ± 0.34	0	2	–	–
25	1.12 ± 0.37	8	**26**	0.60 ± 0.09	0	29	–	–
26	1.45 ± 0.47	34	**29**	1.11 ± 0.37	0	0	–	–
28	1.32 ± 0.08	40	**43**	2.35 ± 1.15	31	17	⩾10	–
29	1.08 ± 0.72	35	**49**	0.94 ± 0.28	0	14	–	–
31	1.16 ± 0.61	25	**77**	0.85 ± 0.34	0	9	–	–
66	1.00 ± 0.19	43	***81***	0.55 ± 0.06	4	19	3.90 ± 0.16	⩾10
70	1.32 ± 0.01	10	***91***	0.77 ± 0.09	11	5	2.83 ± 0.18	⩾10
82	0.94 ± 0.52	21	***95***	1.48 ± 0.63	85	37	0.18 ± 0.01	1.98 ± 0.10
91	1.58 ± 0.66	37	***97***	0.89 ± 0.29	3	9	⩾10*	⩾10*
121	0.59 ± 0.02	27	**107**	0.58 ± 0.09	19	0	–	–
132	0.98 ± 0.15	18	**121**	0.51 ± 0.01	0	3	–	–
141	0.67 ± 0.16	33	**146**	0.54 ± 0.11	0	0	–	–
146	1.27 ± 0.98	13	***157***	1.56 ± 0.48	9	4	9.39 ± 0.90	⩾10
149	0.62 ± 0.08	17	***163***	1.71 ± 0.33	15	0	⩾10*	⩾10*
151	1.71 ± 1.39	nd	**167**	1.24 ± 0.68	4	0	–	–
152	0.91 ± 0.06	31	**178**	0.96 ± 0.59	0	0	–	–
154	0.51 ± 0.01	32	**182**	4.05 ± 0.34	24	8	–	–
156	1.14 ± 0.84	nd	**196**	1.38 ± 0.44	15	24	–	–
158	0.56 ± 0.09	25	**208**	0.85 ± 0.36	6	30	–	–
165	0.99 ± 0.37	nd	**212**	0.71 ± 0.24	2	2	–	–
180	1.88 ± 0.62	25	**214**	0.69 ± 0.21	2	0	–	–
233	0.91 ± 0.55	14	**216**	1.21 ± 0.60	89	36	1.24 ± 0.13	6.71 ± 0.30
245	1.08 ± 0.05	nd	***217***	0.57 ± 0.04	11	0	3.12 ± 0.27	⩾10
346	1.14 ± 0.07	24	**221**	0.57 ± 0.06	7	8	–	–
384	1.17 ± 0.01	nd	**227**	0.85 ± 0.56	0	3	–	–
385	0.92 ± 0.16	nd	**236**	0.72 ± 0.25	10	7	–	–
386	0.96 ± 0.65	15	**238**	0.52 ± 0.06	2	0	–	–
414	1.54 ± 0.08	6	**256**	0.71 ± 0.24	22	5	–	–
429	1.16 ± 0.64	22	**370**	1.78 ± 0.26	79	17	0.83 ± 0.06	6.32 ± 0.53
431	1.18 ± 0.80	nd	**384**	1.75 ± 0.11	7	0	–	–
433	1.58 ± 0.39	0						
436	0.84 ± 0.02	0						
441	1.54 ± 0.48	0						

[a] SD values of three independent experiments at 2 mM; the positive control AMPPNP (DENV Hel) gave a ΔT_m value of 3.46 °C at a concentration of 2 mM; the positive control AdoMet (DENV MTase) gave a ΔT_m value of 6.54 °C at a concentration of 2 mM.
[b] The highest value of two independent measurements measured at 2 mM.
[c] Values are measured at 500 μM.
[d] Values are measured at 1 mM.
[e] IC_{50} values are an average of two to three independent measurements.
* Curves of the IC_{50} determination were impacted by the low solubility of the fragments at high concentration. nd: not determined because of solubility issues.

3. Results and discussion

FBDD strategies identify hot spots in the protein for ligand binding and core fragments which are good starting points for ligand development within novel structural frameworks. In the present study, we have applied a FBS campaign using a combination of biophysical thermal-shift assays (TSA), X-ray crystallography and high-concentration screens on the enzyme activities (HCS), to discover (i) fragments binding and inhibiting DENV Hel and MTase, (ii) novel flavivirus inhibitory sites that can be pursued for further drug design efforts (Fig. 1).

3.1. First-line fragment-based screening by thermal-shift assay

In the FBDD approach, the first step is usually a screening assay of fragment libraries followed by a crystallographic hit validation to find attractive starting points. Accordingly, a library of 500 commercial fragments from Maybridge was firstly designed as to comprise between 7 and 20 non-hydrogen atoms (MW between 100 and 298 g/mol; MW average of 188 g/mol) with the highest structural diversity and including two or more substituents to facilitate analogue synthesis. These 500 fragments were then screened against the NS3 DENV Hel and NS5 DENV MTase proteins using a rapid and inexpensive TSA-based strategy. In TSA, the folding stability of a protein is measured by its thermal-induced unfolding (Nettleship et al., 2008). The interaction of a ligand to a protein can result in the stabilization of this protein that can thereby be identified by an increase in its melting temperature. Because of generally weak affinity of fragments, TSA was performed at a fragment concentration of 2 mM for both DENV Hel and MTase proteins. For all experiments, DMSO and positive controls were used, namely addition of AMPPNP for DENV Hel and AdoMet for DENV MTase assays, for which an increased unfolding temperature is observed, corresponding to positive shifts (ΔT_m) of 3.46 ± 0.4 °C and 6.54 ± 0.7 °C, respectively. All fragments were assayed in duplicate and detection limits were estimated from the screening conditions. Fragment hits were identified as stabilizing the enzymes by at least 0.5 °C in temperature shift. The choice for this cutoff was based on the screening thermal window used for detecting fragment binding in this assay and corresponds to twice the standard deviation of the control sample. Based on this criterion, we identified 36 thermal-shift hits with NS3 DENV4 Hel varying between 0.51 and 1.88 °C and 32 with NS5 DENV3 MTase varying between 0.51 and 4.05 °C, representing a hit rate of 7.2% and 6.6%, respectively (Table 1). All fragment hits were confirmed by re-assaying them under the same conditions. About 200 and 130 fragments displayed a ΔT_m between 0 and 0.5 °C with DENV Hel and MTase, and about 260 and 330 displayed negative ΔT_m values, respectively. This could be due to fragments stabilizing the unfolded state of the protein, or fragments aggregating and causing early destabilization and unfolding of the protein. Due to insufficient solubility under the applied assay conditions 24 fragments were excluded.

The fragment hits listed in Table 1 are mostly six-membered rings (27 out of 62), non-fused bicyclic rings (14 in total), five-membered rings (8 in total) and fused 5–6 membered rings (7 in total), that represent 25%, 37%, 14% and 11% of the fragment library, respectively. A prominent feature for 12 of the 62 resulting hits was the presence of a carboxylate group. At this stage, we attributed this outcome to possible interactions with positively charged residues. One of the larger recorded ΔT_m was for fragment **182** with DENV MTase (4.05 °C, Table 1). In total, six common

Table 2
Crystallographic data and refinement statistics for structures of fragment hits in complex with DENV3 MTase-AdoMet.

	Data collection and phasing statistics						
	81	**91**	**95**	**97**	**157**	**163**	**217**
Resolution range (Å)	185.60–1.52 (1.52–1.52)	61.03–1.52 (1.52–1.52)	186.43–1.63 (1.64–1.63)	61.26–1.53 (1.54–1.53)	183.84–1.60 (1.61–1.60)	184.36–1.61 (1.62–1.61)	185.43–1.47 (1.48–1.47)
No. of unique reflections	90,922 (899)	87,453 (646)	74,604 (741)	88,466 (819)	75,799 (778)	74,916 (591)	92,169 (652)
Completeness (%)	99.9 (99.7)	96.1 (70.6)	100.0 (99.6)	98.6 (93.1)	98.0 (99.7)	97.1 (80.1)	91.9 (66.7)
Multiplicity	4.8 (4.5)	4.2 (2.6)	9.5 (8.8)	3.5 (2.9)	4.5 (4.7)	4.8 (2.4)	3.6 (3.2)
Rmerge[a]	0.062 (0.605)	0.051 (0.478)	0.108 (0.592)	0.057 (0.504)	0.086 (0.613)	0.068 (0.452)	0.047 (0.502)
$I/\sigma(I)$	17.5 (2.3)	19.0 (2.1)	13.9 (3.8)	13.3 (2.1)	13.0 (2.5)	14.2 (2.0)	17.4 (2.3)
	Refinement statistics						
	81	**91**	**95**	**97**	**157**	**163**	**217**
Resolution range (Å)	21.99–1.52 (1.52–1.52)	22.14–1.52 (1.52–1.52)	23.70–1.63 (1.63–1.63)	15.17–1.53 (1.53–1.53)	23.55–1.61 (1.61–1.60)	23.16–1.61 (1.61–1.61)	21.16–1.47 (1.47–1.47)
No. of reflections							
Used for refinement	90,780 (6632)	87,225 (4854)	74,490 (5101)	88,192 (5732)	75,466 (5578)	74,818 (4575)	92,075 (5373)
Used for Rfree calculation	4584 (309)	4476 (230)	3760 (235)	4465 (297)	3837 (290)	3786 (232)	4682 (256)
Water molecules	812	789	718	658	551	507	825
Rwork[b] (%)	16.1	16.7	15.6	17.7	18.8	18.5	16.2
Rfree[c] (%)	18.3	19.4	18.0	20.5	21.9	22.2	18.5
Ligand real space correlation coefficient	0.9282	0.9346	0.9144	0.8434	0.8685	0.8987	0.9127
Rms deviations from ideality							
Bond lengths (Å)	0.010	0.010	0.010	0.010	0.010	0.010	0.010
Bond angles (°)	1.00	0.98	0.98	0.98	0.99	1.01	1.02
Ramanchandran plot							
Residues in most favored regions (%)	98.23	97.83	98.03	97.83	98.03	97.83	98.23
Residues in disallowed regions (%)	0	0.20	0	0.20	0.20	0.20	0

[a] Rmerge = $\Sigma|I_{obs} - I_{av}|/\Sigma I_{av}$, over all symmetry-related observations.
[b] Rwork = $\Sigma|F_{obs} - <|F_{calc}|>|/\Sigma|F_{obs}|$, over all reflections included in the refinement.
[c] Rfree is calculated with 5% of reflections excluded from the refinement. In this formula, $<|F_{calc}|>$ denotes the expectation value of $|F_{calc}|$ under the probability distribution used to define the likelihood function that is maximized in the refinement. Values in parentheses are for the outermost resolution shell of data.

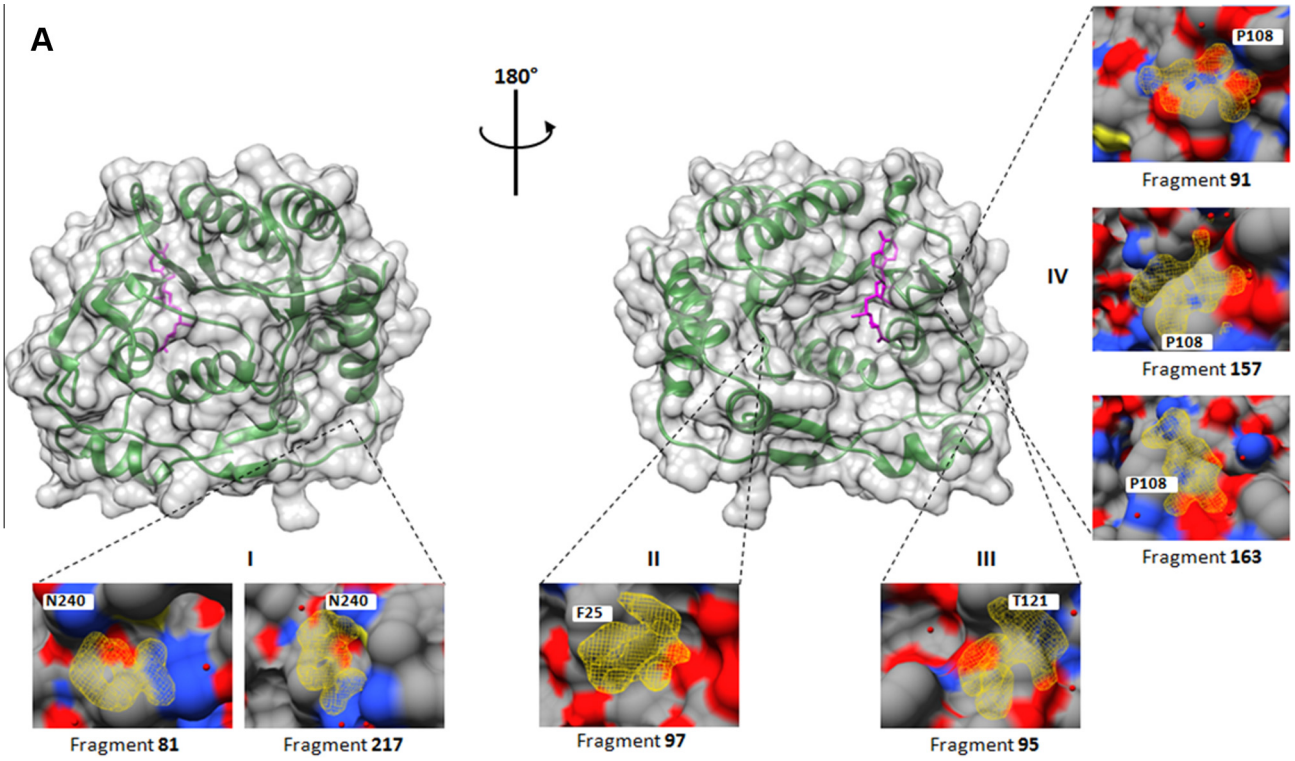

B

Binding site	Fragment	Residues
I	81	L237, N240, R241, R247
	217	L237, N240, R241, R247
II	97	L17, L20, S21, R22, F25
III	95	P115, M116, S117, T121
IV	91	G106, G107, P108, G109, H110, E112
	157	G107, P108, H110, E112
	163	G107, P108, G109, H110, E112

Fig. 2. X-ray crystal structures of seven fragments found to bind the DENV3 MTase. (A) Two opposite views of the DENV3 MTase crystal structure (backbone in green with molecular surface in gray) and AdoMet (shown in magenta) are depicted to localize the four binding sites of fragments **81**, **91**, **95**, **97**, **157**, **163** and **217**. In the insets, F_o–F_c omit electron density maps are shown as a yellow mesh contoured at 1.5σ around the fragments. Carbon atoms are colored in gray, oxygen in red, nitrogen in blue, and sulfur in yellow. Small red spheres represent water molecules around the binding sites. (B) List of DENV3 MTase amino acid residues defining binding sites **I** to **IV**. (For interpretation of the references to color in this figure legend, the reader is referred to the web version of this article.)

fragment hits were identified in both screens, namely **26**, **29**, **91**, **121**, **146** and **384**. These fragments are not part of a distinctive class and cannot be grouped according to their structures that are not listed as known promiscuous binders (Giannetti et al., 2008; Hu and Bajorath, 2010; Mendgen et al., 2012). Although false negatives in initial TSA screens cannot be excluded (Schulz et al., 2012), the strategy appeared efficient and led to the rapid identification of fragment hits that we further confirmed and characterized with crystallography and biochemical assays.

3.2. Fragment-based screening by X-ray crystallography

Structure-based fragment lead discovery strategy needs a well-resolved structure as an entry point into a medicinal chemistry follow-up program. In order to locate the fragment binding sites and gain insight into the nature of protein–ligand interactions, the next step was to conduct structural studies using X-ray crystallography. NS3 DENV Hel and NS5 DENV MTase domains have been readily crystallized as a monomeric free enzyme (Luo et al., 2008) and as a dimeric complex with AdoMet (Lim et al., 2011), respectively, yielding high-resolution X-ray diffraction data. Presence of AdoMet co-purified with MTases from the bacterial lysates has already been widely described (Benarroch et al., 2004; Egloff et al., 2002, 2007; Geiss et al., 2009; Lim et al., 2011; Yap et al., 2010). Since one of the objectives of FBDD is to find new binding sites, we did not attempt to exclude AdoMet from its binding pocket.

The 36 and 32 fragment hits identified by TSA were individually soaked into free DENV4 Hel and DENV3 MTase/AdoMet crystals, between 4 h and overnight. The high DMSO tolerance and robustness of the crystals allowed soaking of fragments at final high concentrations ranging from 10 to 50 mM depending on their solubility, with all yielding high quality X-ray diffraction datasets. Free Hel crystals soaked with selected fragments were obtained, belonging to space group $P4_3$ (cell unit parameters: $a = b = 52$ Å, $c = 193$ Å, $\alpha = \beta = \gamma = 90°$), but all of them failed to show incorporation of the fragments into the crystal structure, despite numerous attempts.

In practice, a major bottleneck of FBDD is the efficient translation of hits obtained from biophysical assays into crystal structures. Indeed, hits can be difficult to translate into structures of protein–ligand complexes for different reasons. It is possible in the first place that the primary screening leads to false positive results. Whether this is the case or not, several scenarios may explain the absence of bound fragments in the structure. It is

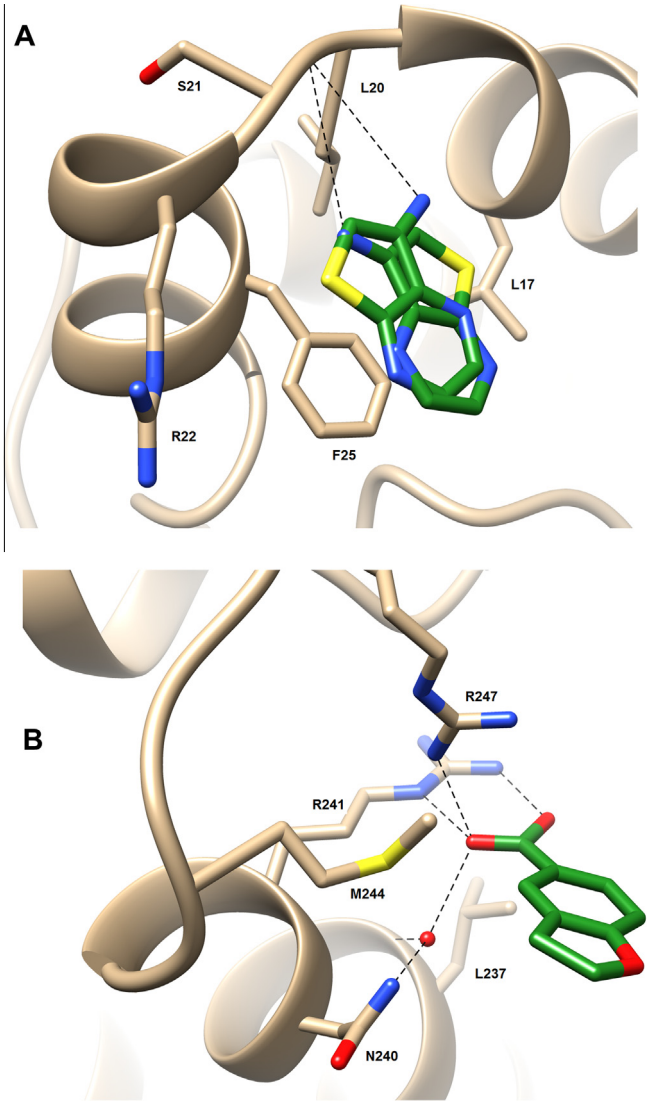

Fig. 3. Crystal structures of DENV-3 MTase in complex with bound fragment hit **97** (**A**) and fragment hit **217** (**B**). Fragments are shown in cylinder representation green carbon atom. Nitrogen, oxygen and sulfur are colored in blue, red and yellow, respectively. Small red spheres represent water molecules around the binding sites. Hydrogen bond interactions are shown as black dotted lines. Amino acid residues shown are those establishing Van der Waals interactions with the fragment hit. (For interpretation of the references to color in this figure legend, the reader is referred to the web version of this article.)

possible that the crystallization conditions (extreme pH, high salt concentrations) impair the interaction between the target and the fragment. Crystal packing interactions can also prevent the compound from accessing its potential binding site if this latter is located at a protein–protein interface. Finally, protein–ligand interactions might induce protein conformational changes in solution whereas the crystal lattice usually locks the protein into a single or a limited set of conformations that might be incompatible with ligand binding. In the case of DENV4 Hel, most of selected fragments inhibit at least the ATPase activity (see Table 1). Nevertheless, we cannot exclude that some false positive hits might have been selected since the inhibition of some compounds is weak. Moreover, DENV4 Hel crystals were obtained near the pH used in the TSA assay and it is unlikely that all the selected fragments target only the interface between the protein molecules in the crystal. Altogether, these observations suggest that fragment binding brings about conformational changes that cannot occur in the crystal, and since the interactions are expected to be poor, crystal soaking with the fragment hits has no effect on crystal lattice interactions. Indeed, the structure of a complex of DENV Hel with AMP-PNP was obtained by co-crystallization and not crystal soaking. Interestingly, DENV Hel is a very dynamic enzyme (Luo et al., 2008). Crystals made of DENV Hel in complex with RNA can accommodate AMPPNP by soaking. The presence of RNA induces a rearrangement of the quaternary structure that therefore enlarges the RNA binding site and modifies the ATP binding cleft. Moreover, flaviviral helicases can adopt several conformations depending on the crystallization conditions and the expressed constructs (with or without the protease domain) (Assenberg et al., 2009; Luo et al., 2010; Xu et al., 2006). All these reported studies demonstrate that DENV Hel can undergo local or long-range rearrangements depending on the presence of ligands, on the protein conditions and on the exact constructs used, suggesting that the single conformation adopted by the protein in the "free" crystal has a low probability of being well adapted to the screening of protein–ligand interactions by the soaking method. Co-crystallization could be used as an alternative to soaking in order to obtain protein–ligand complexes amenable to X-ray crystallography, but the throughput of the procedure would be greatly reduced and the approach would become unsuitable for the discovery of large numbers of fragment hits.

DENV3 MTase/AdoMet crystals soaked with selected fragments were obtained in space group $P2_12_12$ (cell unit parameters: a = 61 Å, b = 185 Å, c = 51 Å, $\alpha = \beta = \gamma = 90°$) with two protein molecules in the asymmetric unit. We were able to identify reliable electron density corresponding to the soaked compound for 7 out of the 32 fragments studied (~22% of the total), with resolutions for the final refined structures in the 1.47–1.63 Å range and high quality Rwork and Rfree values and, importantly, with high ligand real-space correlation coefficients. Data collection and refinement statistics for the seven hit crystal structures are given in Table 2. All fragment hits from X-ray crystallography were subsequently verified by repeating the experiments. However, we were unable to obtain a crystal structure complex for the fragment hit with the largest recorded ΔT_m (fragment **182**, 4.05 °C, Table 1) from the TSA screening campaign, even while performing co-crystallization experiments. The surface representation of DENV MTase along with F_o–F_c maps displaying the ligand density for the seven hits are shown in Fig. 2 summarizing the binding interfaces and illustrating the presence of low-energy water molecules involved in efficient fragment binding. The structural details concerning two of these fragments (fragment **97** PDB code 4ctk and fragment **217** PDB code 4ctj) will be depicted here.

Briefly, the core structure of DENV MTase consists of a 7-stranded β-sheet surrounded by four α-helices (Egloff et al., 2002). Three distinct functional binding sites have been identified: (i) the AdoHcy/AdoMet binding site serving as the AdoMet-binding pocket during the methylation reactions, (ii) the GTP-binding site which allows the specific recognition of the RNA cap-structure and (iii) the RNA-binding site formed by a highly conserved and positively charged groove. Analysis of the crystal structures indicated that, among the seven fragment hits, four different binding sites (**I–IV)** could be defined, which are depicted in Fig. 2, one overlapping with the GTP-binding site (site **II** with fragment **97** bound in two different orientations to the GTP-binding site through π-stacking interactions) and three novel binding sites (site **I** with fragments **81** and **217**, site **III** with fragment **95** and site **IV** with fragments **91**, **157** and **163**) that will be explored for future DENV MTase inhibitors.

As shown in Fig. 3, fragment **97** (thieno[2,3-b]pyrazin-7-amine), bound in two different orientations to the GTP-binding site **II**, is mainly stabilized by face-to-face π-interactions with Phe25 from chain A. Additionally, the nitrogen atom N1 (for the two different orientations) makes hydrogen-bonding interactions with the

backbone carbonyl of Leu17 with 2.84 and 3.14 Å distance, and Leu20 with 2.98 and 3.45 Å distance. All other contacts are Van der Waals interactions and involve side chains of residues Leu17, Leu20 and Arg22. A second fragment **97** stacks with the first one (not shown in Fig. 3, see PDB code 4ctk) but its presence is not significant since it does not bind to the protein.

Fragment **217** (2,3-dihydrobenzo[b]furan-5-carboxylic acid) was observed at site **I** making ionic interactions between its carboxylic acid moiety and the guanidinium groups of Arg241 and Arg247 with 2.79 and 2.63 Å distance, respectively. Additionally, the formation of a hydrogen-bonded water bridge also stabilizes fragment **217** and involves the nitrogen of the amide side chain of Asn240, as well as the oxygen atom of the amide backbone of Leu237.

For the other fragments identified, we observed both hydrophobic packing as well as specific hydrogen-bond interactions with either crystallographic water, target residues or water-mediated interactions with target residues.

Our successful FBS-X campaign on DENV MTase took four months. Recent developments in hardware and improvement in data collection at synchrotron beamlines allowed high quality data to be collected more rapidly. Moreover, the use of Pipedream (see Section 2) reduced significantly the X-ray structure solution and hit identification times.

3.3. Validation and characterization of fragment hits by enzymatic assays

To confirm and further characterize the fragment hits identified by TSA and FBS-X, and to prioritize the fragment hits for follow-up chemistry and optimization, we next performed enzymatic assays to assess the inhibitory activity of these fragments on DENV Hel ATPase, N7- and 2′-*O*-MTase. Because of the generally weak affinity of fragments, the assays were carried out at high compound concentrations (500 μM to 1 mM range).

ATPase inhibition assays were performed in order to validate the primary fragment screening by TSA. The results summarized in Table 1 show that 11 out of 36 fragment hits have a significant effect on ATPase assay, with inhibition potency higher than 25% at 2 mM. Nevertheless, none of them reach 50% inhibition. These results enabled the validation of the TSA screening. However, since no co-structure was obtained for DENV Hel, the functional study with fragment hits identified by TSA screening was not pursued further.

In DENV N7- and 2′-*O*-MTase assays, which measure the inhibition of [^{3}H]-AdoMet incorporation into viral mRNA cap (Barral et al., 2013), all fragments were assayed in duplicate. We compared the DENV 2′-*O*-MTase inhibition (methylation of substrate $^{7Me}GpppAC_4$ resulting in $^{7Me}Gppp_{2'OMe}AC_4$) to DENV N7-MTase inhibition (methylation of substrate $GpppA_{2'OMe}$-RNA_{74} resulting in $^{7Me}GpppA_{2'OMe}$-RNA_{74}). As shown in Table 1 and Fig. 4 and 29 fragments weakly inhibit both N7- and 2′-*O*-MTase activities (less than 30%) at a concentration of 1 mM and 500 μM, respectively. Fragments **95** and **216** show more potent inhibition of both N7- and 2′-*O*-MTase activities, while fragment **370** inhibits more efficiently 2′-*O*-MTase activity (79%) but show limited (17%) inhibition of N7-MTase activity.

Fragments with a percentage of inhibition greater than 30%, as well as fragments discovered in the crystallographic screen, were confirmed by IC_{50} value determination for both N7- and 2′-*O*-MTase activities (Table 1 and Fig. 5). In total, four fragments (**43**, **95**, **216** and **370**) inhibit at least one of the two MTase activities at more than 30%. Only one of them (fragment **95**) was discovered by FBS-X. As expected, dose response curves indicate that fragments **95** (Fig. 5), **216** and **370** inhibit both 2′-*O*- and N7-MTase activities but show a 5–11-fold stronger inhibition of 2′-*O*-MTase compared to N7-MTase activity, with IC_{50} values in the micromolar to the submillimolar range (Table 1). Fragments **81**, **91**, **157** and **217** inhibit only the 2′-*O*-MTase activity with IC_{50} values in the submillimolar range. However, IC_{50} values for fragments **43**, **97** and **163** were too weak to be measured ($\geqslant$10 mM) and aggregation was detected at high concentration.

As described previously, fragment screening by X-ray crystallography revealed three new and promising binding sites within DENV MTase, since they were found to be inhibitory of at least one of the two activities, whereas fragment **97** binding to the GTP-binding site and **163** display a relatively weak IC_{50}. It is worth noting that compounds displaying low inhibition rates can penetrate into the crystals and reveal their successful binding in a crystal structure.

Furthermore, out of the 32 fragments identified as hits by the first TSA screen, two of them, fragments **216** and **370**, which inhibit both MTase activities with IC_{50} values ranging from 830 μM to 6.7 mM, were not observed to bind to the DENV MTase protein crystals in soaking or co-crystallization experiments. It is remarkable that according to these results, no obvious correlation

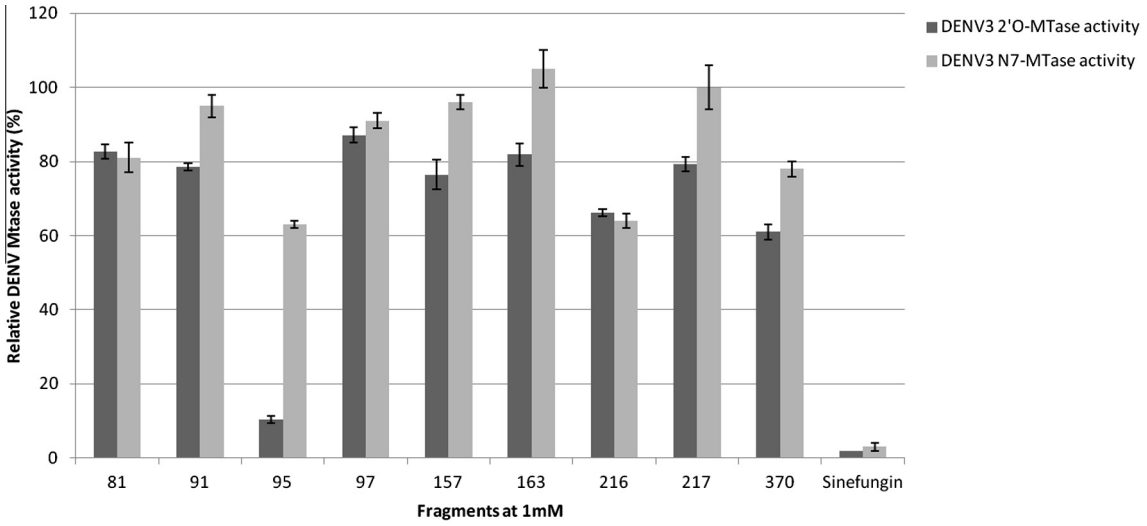

Fig. 4. Inhibition of DENV3 N7- and 2′-*O*-MTase activities by 9 fragment hits and Sinefungin as positive control. DENV3 MTase was incubated with $GpppA_{2'OMe}$-RNA_{74} (for N7-MTase activity), $^{7Me}GpppAC_4$ (for 2′-*O*-MTase activity) and [^{3}H]AdoMet in the presence of 1 mM of each fragment candidate as given in Section 2. Error bars represent SD values of two to three independent experiments.

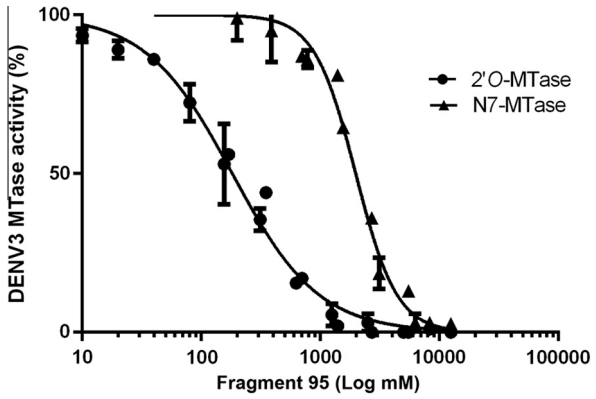

Fig. 5. Example of dose-dependent inhibition curves of DENV3 N7- and 2′-*O*-MTase activities by fragment **95**.

between potency observed in the enzymatic assay and probability to obtain a crystal structure can be established. In that respect, the optimization of poorly active inhibitors should nevertheless be pursued to optimize their binding properties since they can affect functions other than the protein enzymatic activities such as protein/protein interactions involved in the formation of the replication complex.

FBDD using *in silico* screening approaches (Chen et al., 2009; Ekonomiuk et al., 2009a,b; Karelson et al., 2012; Knehans et al., 2011) and/or focused libraries (Ismail et al., 2012; Schoenfeld et al., 2013; Stammers et al., 2013; Steuer et al., 2011; Talamas et al., 2013; Wyss et al., 2004) have already been applied to targets from RNA viruses. Nevertheless, these strategies have the major disadvantage of selecting *a priori* binding site(s) and therefore cannot lead to the discovery of original allosteric sites. Our study aimed at demonstrating the application of a random fragment-based screening strategy for new anti-flaviviral hits and related binding sites identification. The strategy was tested on two targets involved in the replication of Dengue virus, DENV Hel and MTase. Although hits were obtained from the primary screening (*e.g.* TSA) for both targets, only the MTase responded well to the downstream crystal soaking, leading to the discovery of three novel binding sites and seven fragment hits.

To our knowledge, only one example of random FBS has been conducted on an RNA virus target (Antonysamy et al., 2008), namely HCV NS5b polymerase. In this study, the first-line screening relied on crystal soaking with fragment cocktails. About 2% of fragment hits were identified, in line with our results for DENV MTase. Nevertheless, our use of TSA as first-line screening has greatly reduced efforts in crystallization, soaking and data analysis. In the time course of this study, new high resolution structures of DENV NS5 RdRp (Lim et al., 2013a) and NS3 protease (Noble et al., 2012) have been published opening new perspectives for random FBDD against Dengue virus.

The fragment hits identified against DENV MTase provide a starting point for the development of larger, higher affinity molecules that bind to allosteric sites. Thus, these results lay the structural foundation for the development of a new class of flaviviral inhibitors. The development of these allosteric fragments into high-affinity allosteric inhibitors will be pursued in the next stage of this research project, with the guidance provided by virtual *in silico* docking/modelling to help decision making for further optimization of fragments by medicinal chemistry.

Acknowledgements

We wish to thank Julie Lichière and Joelle Boretto-Soler for technical assistance, and Françoise Debart for providing short capped RNAs. We especially thank Miguel Ortiz-Lombardia for helpful discussions and his teaching in crystallography. We are also grateful to Bruno Canard for his support in this project. This work was supported by the project SILVER (Health-F3-2010-260644) of the European Union 7th Framework Program and by the French National Agency for Research (ANR-13-JS07-0006-01).

References

Abad-Zapatero, C., 2007. Ligand efficiency indices for effective drug discovery. Expert Opin. Drug Discov. 2, 469–488.
Antonysamy, S.S., Aubol, B., Blaney, J., Browner, M.F., Giannetti, A.M., Harris, S.F., Hebert, N., Hendle, J., Hopkins, S., Jefferson, E., Kissinger, C., Leveque, V., Marciano, D., McGee, E., Najera, I., Nolan, B., Tomimoto, M., Torres, E., Wright, T., 2008. Fragment-based discovery of hepatitis C virus NS5b RNA polymerase inhibitors. Bioorg. Med. Chem. Lett. 18, 2990–2995.
Assenberg, R., Mastrangelo, E., Walter, T.S., Verma, A., Milani, M., Owens, R.J., Stuart, D.I., Grimes, J.M., Mancini, E.J., 2009. Crystal structure of a novel conformational state of the flavivirus NS3 protein: implications for polyprotein processing and viral replication. J. Virol. 83, 12895–12906.
Barral, K., Sallamand, C., Petzold, C., Coutard, B., Collet, A., Thillier, Y., Zimmermann, J., Vasseur, J.J., Canard, B., Rohayem, J., Debart, F., Decroly, E., 2013. Development of specific dengue virus 2′-*O*- and N7-methyltransferase assays for antiviral drug screening. Antiviral Res. 99, 292–300.
Bembenek, S.D., Tounge, B.A., Reynolds, C.H., 2009. Ligand efficiency and fragment-based drug discovery. Drug Discov. Today 14, 278–283.
Benarroch, D., Egloff, M.P., Mulard, L., Guerreiro, C., Romette, J.L., Canard, B., 2004a. A structural basis for the inhibition of the NS5 dengue virus mRNA 2′-*O*-methyltransferase domain by ribavirin 5′-triphosphate. J. Biol. Chem. 279, 35638–35643.
Benarroch, D., Selisko, B., Locatelli, G.A., Maga, G., Romette, J.L., Canard, B., 2004b. The RNA helicase, nucleotide 5′-triphosphatase, and RNA 5′-triphosphatase activities of Dengue virus protein NS3 are Mg2+-dependent and require a functional Walker B motif in the helicase catalytic core. Virology 328, 208–218.
Bollati, M., Alvarez, K., Assenberg, R., Baronti, C., Canard, B., Cook, S., Coutard, B., Decroly, E., de Lamballerie, X., Gould, E.A., Grard, G., Grimes, J.M., Hilgenfeld, R., Jansson, A.M., Malet, H., Mancini, E.J., Mastrangelo, E., Mattevi, A., Milani, M., Moureau, G., Neyts, J., Owens, R.J., Ren, J., Selisko, B., Speroni, S., Steuber, H., Stuart, D.I., Unge, T., Bolognesi, M., 2010. Structure and functionality in flavivirus NS-proteins: perspectives for drug design. Antiviral Res. 87, 125–148.
Bricogne, G., Blanc, E., Brandl, M., Flensburg, C., Keller, P., Paciorek, W., Roversi, P., Sharff, A., Smart, O.S., Vonrhein, C., Womack, T.O., 2011. BUSTER Version 2.11.2. Global Phasing Ltd., Cambridge, United Kingdom.
Bruno, I.J., Cole, J.C., Kessler, M., Luo, J., Motherwell, W.D., Purkis, L.H., Smith, B.R., Taylor, R., Cooper, R.I., Harris, S.E., Orpen, A.G., 2004. Retrieval of crystallographically-derived molecular geometry information. J. Chem. Inf. Comput. Sci. 44, 2133–2144.
Byrd, C.M., Grosenbach, D.W., Berhanu, A., Dai, D., Jones, K.F., Cardwell, K.B., Schneider, C., Yang, G., Tyavanagimatt, S., Harver, C., Wineinger, K.A., Page, J., Stavale, E., Stone, M.A., Fuller, K.P., Lovejoy, C., Leeds, J.M., Hruby, D.E., Jordan, R., 2013. Novel benzoxazole inhibitor of dengue virus replication that targets the NS3 helicase. Antimicrob. Agents Chemother. 57, 1902–1912.
Chen, C.S., Chiou, C.T., Chen, G.S., Chen, S.C., Hu, C.Y., Chi, W.K., Chu, Y.D., Hwang, L.H., Chen, P.J., Chen, D.S., Liaw, S.H., Chern, J.W., 2009. Structure-based discovery of triphenylmethane derivatives as inhibitors of hepatitis C virus helicase. J. Med. Chem. 52, 2716–2723.
Ciulli, A., Abell, C., 2007. Fragment-based approaches to enzyme inhibition. Curr. Opin. Biotechnol. 18, 489–496.
Congreve, M., Chessari, G., Tisi, D., Woodhead, A.J., 2008. Recent developments in fragment-based drug discovery. J. Med. Chem. 51, 3661–3680.
Daffis, S., Szretter, K.J., Schriewer, J., Li, J., Youn, S., Errett, J., Lin, T.Y., Schneller, S., Zust, R., Dong, H., Thiel, V., Sen, G.C., Fensterl, V., Klimstra, W.B., Pierson, T.C., Buller, R.M., Gale Jr., M., Shi, P.Y., Diamond, M.S., 2010. 2′-*O* methylation of the viral mRNA cap evades host restriction by IFIT family members. Nature 468, 452–456.
Davis, I.W., Leaver-Fay, A., Chen, V.B., Block, J.N., Kapral, G.J., Wang, X., Murray, L.W., Arendall III, W.B., Snoeyink, J., Richardson, J.S., Richardson, D.C., 2007. MolProbity: all-atom contacts and structure validation for proteins and nucleic acids. Nucleic Acids Res. 35, W375–W383.
de Kloe, G.E., Bailey, D., Leurs, R., de Esch, I.J., 2009. Transforming fragments into candidates: small becomes big in medicinal chemistry. Drug Discov. Today 14, 630–646.
Delean, A., Munson, P.J., Rodbard, D., 1978. Simultaneous analysis of families of sigmoidal curves – application to bioassay, radioligand assay, and physiological dose-response curves. Am. J. Physiol. 235, E97–E102.
Dong, H.P., Zhang, B., Shi, P.Y., 2008. Flavivirus methyltransferase: a novel antiviral target. Antiviral Res. 80, 1–10.
Dong, H.P., Chang, D.C., Xie, X.P., Toh, Y.X., Chung, K.Y., Zou, G., Lescar, J., Lim, S.P., Shi, P.Y., 2010. Biochemical and genetic characterization of dengue virus methyltransferase. Virology 405, 568–578.
Egloff, M.P., Benarroch, D., Selisko, B., Romette, J.L., Canard, B., 2002. An RNA cap (nucleoside-2′-*O*-)-methyltransferase in the flavivirus RNA polymerase NS5: crystal structure and functional characterization. EMBO J. 21, 2757–2768.

Egloff, M.P., Decroly, E., Malet, H., Selisko, B., Benarroch, D., Ferron, F., Canard, B., 2007. Structural and functional analysis of methylation and 5′-RNA sequence requirements of short capped RNAs by the methyltransferase domain of dengue virus NS5. J. Mol. Biol. 372, 723–736.

Ekonomiuk, D., Su, X.C., Ozawa, K., Bodenreider, C., Lim, S.P., Otting, G., Huang, D., Caflisch, A., 2009a. Flaviviral protease inhibitors identified by fragment-based library docking into a structure generated by molecular dynamics. J. Med. Chem. 52, 4860–4868.

Ekonomiuk, D., Su, X.C., Ozawa, K., Bodenreider, C., Lim, S.P., Yin, Z., Keller, T.H., Beer, D., Patel, V., Otting, G., Caflisch, A., Huang, D., 2009b. Discovery of a non-peptidic inhibitor of west nile virus NS3 protease by high-throughput docking. PLoS Negl. Trop. Dis, 3, e356.

Emsley, P., Lohkamp, B., Scott, W.G., Cowtan, K., 2010. Features and development of Coot. Acta Crystallogr. D Biol. Crystallogr. 66, 486–501.

Erlanson, D.A., 2012. Introduction to fragment-based drug discovery. Top. Curr. Chem. 317, 1–32.

Evans, P., 2006. Scaling and assessment of data quality. Acta Crystallogr. D Biol. Crystallogr. 62, 72–82.

Geiss, B.J., Thompson, A.A., Andrews, A.J., Sons, R.L., Gari, H.H., Keenan, S.M., Peersen, O.B., 2009. Analysis of flavivirus NS5 methyltransferase cap binding. J. Mol. Biol. 385, 1643–1654.

Giannetti, A.M., Koch, B.D., Browner, M.F., 2008. Surface plasmon resonance based assay for the detection and characterization of promiscuous inhibitors. J. Med. Chem. 51, 574–580.

Hajduk, P.J., Greer, J., 2007. A decade of fragment-based drug design: strategic advances and lessons learned. Nat. Rev. Drug Discov. 6, 211–219.

Henkel, R.D., VandeBerg, J.L., Walsh, R.A., 1988. A microassay for ATPase. Anal. Biochem. 169, 312–318.

Hopkins, A.L., Groom, C.R., Alex, A., 2004. Ligand efficiency: a useful metric for lead selection. Drug Discov. Today 9, 430–431.

Hu, Y., Bajorath, J., 2010. Molecular scaffolds with high propensity to form multi-target activity cliffs. J. Chem. Inf. Model. 50, 500–510.

Ismail, M.A., Abou El Ella, D.A., Abouzid, K.A., Mahmoud, A.H., 2012. Integrated structure-based activity prediction model of benzothiadiazines on various genotypes of HCV NS5b polymerase (1a, 1b and 4) and its application in the discovery of new derivatives. Bioorg. Med. Chem. 20, 2455–2478.

Kabsch, W., 2010. Xds. Acta Crystallogr. D Biol. Crystallogr. 66, 125–132.

Karelson, M., Dobchev, D.A., Karelson, G., Tamm, T., Tamm, K., Nikonov, A., Mutso, M., Merits, A., 2012. Fragment-based development of HCV protease inhibitors for the treatment of hepatitis C. Curr. Comput. Aided Drug Des. 8, 55–61.

Knehans, T., Schuller, A., Doan, D.N., Nacro, K., Hill, J., Guntert, P., Madhusudhan, M.S., Weil, T., Vasudevan, S.G., 2011. Structure-guided fragment-based in silico drug design of dengue protease inhibitors. J. Comput. Aided Mol. Des. 25, 263–274.

Kuo, L.C., 2011. Fragment-based drug design – tools, practical approaches, and examples. Preface. Methods Enzymol. 493, xxi–xxii.

Lantez, V., Dalle, K., Charrel, R., Baronti, C., Canard, B., Coutard, B., 2011. Comparative production analysis of three phlebovirus nucleoproteins under denaturing or non-denaturing conditions for crystallographic studies. PLoS Negl. Trop. Dis. 5, e936.

Lim, S.P., Sonntag, L.S., Noble, C., Nilar, S.H., Ng, R.H., Zou, G., Monaghan, P., Chung, K.Y., Dong, H.P., Liu, B.P., Bodenreider, C., Lee, G., Ding, M., Chan, W.L., Wang, G., Jian, Y.L., Chao, A.T., Lescar, J., Yin, Z., Vedananda, T.R., Keller, T.H., Shi, P.Y., 2011. Small molecule inhibitors that selectively block dengue virus methyltransferase. J. Biol. Chem. 286, 6233–6240.

Lim, S.P., Koh, J.H., Seh, C.C., Liew, C.W., Davidson, A.D., Chua, L.S., Chandrasekaran, R., Cornvik, T.C., Shi, P.Y., Lescar, J., 2013a. A crystal structure of the dengue virus non-structural protein 5 (ns5) polymerase delineates interdomain amino acid residues that enhance its thermostability and de novo initiation activities. J. Biol. Chem. 288, 31105–31114.

Lim, S.P., Wang, Q.Y., Noble, C.G., Chen, Y.L., Dong, H., Zou, B., Yokokawa, F., Nilar, S., Smith, P., Beer, D., Lescar, J., Shi, P.Y., 2013b. Ten years of dengue drug discovery: progress and prospects. Antiviral Res. 100, 500–519.

Lundqvist, T., 2005. The devil is still in the details – driving early drug discovery forward with biophysical experimental methods. Curr. Opin. Drug Discov. Devel. 8, 513–519.

Luo, D., Xu, T., Hunke, C., Gruber, G., Vasudevan, S.G., Lescar, J., 2008. Crystal structure of the NS3 protease-helicase from dengue virus. J. Virol. 82, 173–183.

Luo, D., Wei, N., Doan, D.N., Paradkar, P.N., Chong, Y., Davidson, A.D., Kotaka, M., Lescar, J., Vasudevan, S.G., 2010. Flexibility between the protease and helicase domains of the dengue virus NS3 protein conferred by the linker region and its functional implications. J. Biol. Chem. 285, 18817–18827.

Mastrangelo, E., Pezzullo, M., De Burghgraeve, T., Kaptein, S., Pastorino, B., Dallmeier, K., de Lamballerie, X., Neyts, J., Hanson, A.M., Frick, D.N., Bolognesi, M., Milani, M., 2012. Ivermectin is a potent inhibitor of flavivirus replication specifically targeting NS3 helicase activity: new prospects for an old drug. J. Antimicrob. Chemother. 67, 1884–1894.

McCoy, A.J., Grosse-Kunstleve, R.W., Adams, P.D., Winn, M.D., Storoni, L.C., Read, R.J., 2007. Phaser crystallographic software. J. Appl. Crystallogr. 40, 658–674.

Mendgen, T., Steuer, C., Klein, C.D., 2012. Privileged scaffolds or promiscuous binders: a comparative study on rhodanines and related heterocycles in medicinal chemistry. J. Med. Chem. 55, 743–753.

Milani, M., Mastrangelo, E., Bollati, M., Selisko, B., Decroly, E., Bouvet, M., Canard, B., Bolognesi, M., 2009. Flaviviral methyltransferase/RNA interaction: structural basis for enzyme inhibition. Antiviral Res. 83, 28–34.

Murray, C.W., Rees, D.C., 2009. The rise of fragment-based drug discovery. Nat. Chem. 1, 187–192.

Nettleship, J.E., Brown, J., Groves, M.R., Geerlof, A., 2008. Methods for protein characterization by mass spectrometry, thermal shift (ThermoFluor) assay, and multiangle or static light scattering. Methods Mol. Biol. 426, 299–318.

Noble, C.G., Seh, C.C., Chao, A.T., Shi, P.Y., 2012. Ligand-bound structures of the dengue virus protease reveal the active conformation. J. Virol. 86, 438–446.

Papageorgiou, N., Coutard, B., Lantez, V., Gautron, E., Chauvet, O., Baronti, C., Norder, H., de Lamballerie, X., Heresanu, V., Ferte, N., Veesler, S., Gorbalenya, A.E., Canard, B., 2010. The 2C putative helicase of echovirus 30 adopts a hexameric ring-shaped structure. Acta Crystallogr. D Biol. Crystallogr. 66, 1116–1120.

Schoenfeld, R.C., Bourdet, D.L., Brameld, K.A., Chin, E., de Vicente, J., Fung, A., Harris, S.F., Lee, E.K., Le Pogam, S., Leveque, V., Li, J., Lui, A.S., Najera, I., Rajyaguru, S., Sangi, M., Steiner, S., Talamas, F.X., Taygerly, J.P., Zhao, J., 2013. Discovery of a novel series of potent non-nucleoside inhibitors of hepatitis C virus NS5B. J. Med. Chem. 56, 8163–8182.

Schulz, M.N., Landstrom, J., Hubbard, R.E., 2012. MTSA – a Matlab program to fit thermal shift data. Anal. Biochem. 433, 43–47.

Scott, D.E., Coyne, A.G., Hudson, S.A., Abell, C., 2012. Fragment-based approaches in drug discovery and chemical biology. Biochemistry 51, 4990–5003.

Selisko, B., Peyrane, F.F., Canard, B., Alvarez, K., Decroly, E., 2010. Biochemical characterization of the (nucleoside-2′O)-methyltransferase activity of dengue virus protein NS5 using purified capped RNA oligonucleotides (7Me)GpppAC(n) and GpppAC(n). J. Gen. Virol. 91, 112–121.

Sharff, A., Keller, P., Vonrhein, C., Smart, O., Womack, T., Flensburg, C., Paciorek, C., Bricogne, G., 2011. Pipedream, Version 0.1.4. Global Phasing Ltd., Cambridge, United Kingdom.

Siegal, G., Ab, E., Schultz, J., 2007. Integration of fragment screening and library design. Drug Discov. Today 12, 1032–1039.

Smart, O.S., Womack, T.O., Sharff, A., Flensburg, C., Keller, P., Paciorek, W., Vonrhein, C., Bricogne, G., 2011. Grade, Version 1.1.1. Global Phasing Ltd., Cambridge, United Kingdom.

Stammers, T.A., Coulombe, R., Rancourt, J., Thavonekham, B., Fazal, G., Goulet, S., Jakalian, A., Wernic, D., Tsantrizos, Y., Poupart, M.A., Bos, M., McKercher, G., Thauvette, L., Kukolj, G., Beaulieu, P.L., 2013. Discovery of a novel series of non-nucleoside thumb pocket 2 HCV NS5B polymerase inhibitors. Bioorg. Med. Chem. Lett. 23, 2585–2589.

Steuer, C., Gege, C., Fischl, W., Heinonen, K.H., Bartenschlager, R., Klein, C.D., 2011. Synthesis and biological evaluation of alpha-ketoamides as inhibitors of the Dengue virus protease with antiviral activity in cell-culture. Bioorg. Med. Chem. 19, 4067–4074.

Talamas, F.X., Ao-Ieong, G., Brameld, K.A., Chin, E., de Vicente, J., Dunn, J.P., Ghate, M., Giannetti, A.M., Harris, S.F., Labadie, S.S., Leveque, V., Li, J., Lui, A.S., McCaleb, K.L., Najera, I., Schoenfeld, R.C., Wang, B., Wong, A., 2013. De novo fragment design: a medicinal chemistry approach to fragment-based lead generation. J. Med. Chem. 56, 3115–3119.

Thomas, S.J., Endy, T.P., 2013. Current issues in dengue vaccination. Curr. Opin. Infect. Dis. 26, 429–434.

Vonrhein, C., Flensburg, C., Keller, P., Sharff, A., Smart, O., Paciorek, W., Womack, T., Bricogne, G., 2011. Data processing and analysis with the autoPROC toolbox. Acta Crystallogr. D Biol. Crystallogr. 67, 293–303.

Womack, T., Smart, O., Sharff, A., Flensburg, C., Keller, P., Paciorek, W., Vonrhein, C., Bricogne, G., 2011. Rhofit, Version 1.2.3. Global Phasing Ltd., Cambridge, United Kingdom.

Wyss, D.F., Arasappan, A., Senior, M.M., Wang, Y.S., Beyer, B.M., Njoroge, F.G., McCoy, M.A., 2004. Non-peptidic small-molecule inhibitors of the single-chain hepatitis C virus NS3 protease/NS4A cofactor complex discovered by structure-based NMR screening. J. Med. Chem. 47, 2486–2498.

Xu, T., Sampath, A., Chao, A., Wen, D., Nanao, M., Chene, P., Vasudevan, S.G., Lescar, J., 2005. Structure of the Dengue virus helicase/nucleoside triphosphatase catalytic domain at a resolution of 2.4 A. J. Virol. 79, 10278–10288.

Xu, T., Sampath, A., Chao, A., Wen, D., Nanao, M., Luo, D., Chene, P., Vasudevan, S.G., Lescar, J., 2006. Towards the design of flavivirus helicase/NTPase inhibitors: crystallographic and mutagenesis studies of the dengue virus NS3 helicase catalytic domain. Novartis Found. Symp. 277, 87–97.

Yap, L.J., Luo, D., Chung, K.Y., Lim, S.P., Bodenreider, C., Noble, C., Shi, P.Y., Lescar, J., 2010. Crystal structure of the dengue virus methyltransferase bound to a 5′-capped octameric RNA. PLoS ONE 5.

Yon, C., Teramoto, T., Mueller, N., Phelan, J., Ganesh, V.K., Murthy, K.H., Padmanabhan, R., 2005. Modulation of the nucleoside triphosphatase/RNA helicase and 5′-RNA triphosphatase activities of Dengue virus type 2 nonstructural protein 3 (NS3) by interaction with NS5, the RNA-dependent RNA polymerase. J. Biol. Chem. 280, 27412–27419.

Zust, R., Cervantes-Barragan, L., Habjan, M., Maier, R., Neuman, B.W., Ziebuhr, J., Szretter, K.J., Baker, S.C., Barchet, W., Diamond, M.S., Siddell, S.G., Ludewig, B., Thiel, V., 2011. Ribose 2′-*O*-methylation provides a molecular signature for the distinction of self and non-self mRNA dependent on the RNA sensor Mda5. Nat. Immunol. 12, 137–143.

Zust, R., Dong, H., Li, X.F., Chang, D.C., Zhang, B., Balakrishnan, T., Toh, Y.X., Jiang, T., Li, S.H., Deng, Y.Q., Ellis, B.R., Ellis, E.M., Poidinger, M., Zolezzi, F., Qin, C.F., Shi, P.Y., Fink, K., 2013. Rational design of a live attenuated dengue vaccine: 2′-*O*-methyltransferase mutants are highly attenuated and immunogenic in mice and macaques. PLoS Pathog. 9, e1003521.